Organic Photovoltaic Devices with Colloidal TiO_2 Nanorods as Key Functional Components

Anna Loiudice, [a,b] Aurora Rizzo, *[c] Luisa De Marco, [b] Maria R. Belviso, [d] Gianvito Caputo, [c] P. Davide Cozzoli, [a,c] and Giuseppe Gigli [a,c]

We report on a novel approach to integrate colloidal anatase TiO_2 nanorods as key functional components into polymer bulk heterojunction (BHJ) photovoltaic devices by means of mild, all-solution-based processing techniques. The successful integration of colloidal nanoparticles in organic solar cells relies on the ability to remove the long chain insulating ligands, which indeed severely reduces the charge transport. To this aim we have exploited the concomitant mechanisms of UV-light-driven photocatalytic removal of adsorbed capping ligands and hydrophylicization of TiO_2 surfaces in both solid-state and liquid-phase conditions. We have demonstrated the successful integration of the UV-irradiated films and colloidal solutions of TiO_2 nanorods in inverted and conventional solar cells geometries respectively. The inverted devices show a power conversion efficiency of 2.3% that is *ca.* three times improvement over their corresponding cell counterpart incorporating untreated TiO_2, demonstrating the excellent electron-collecting property of the UV-irradiated TiO_2 films. The integration of UV- treated TiO_2 solutions in conventional devices results in doubled power conversion efficiency for the thinner active layer and in maximum power conversion efficiency of 2.8% for 110 nm thick device. In addition, we have demonstrated, with the support of device characterizations and optical simulations that the TiO_2 nanocrystal buffer layer acts both as the electron-transporting/hole-blocking material and optical spacer.

Introduction

In the past decade organic bulk heterojunction photovoltaic (OPV) cells fabricated from polymers[1] and small molecule[2] have attracted significant interest in academic and industrial communities because of their technological potential for the realization of low-cost, printable, lightweight, large-area and flexible devices.[3,4]

To improve the performance of organic photovoltaic cells, disparate strategies have been pursued, including the development of new low-band-gap materials capable of harvesting a broader range of solar wavelengths,[5,6] advanced methods to control the morphology of active film layers as a means of improving charge transport and reducing recombination,[7] and the construction of novel device architectures for tandem[8,9] and inverted cells[10]. In addition, the optimization of charge collection efficiency and interfacial stability at the organic layer/electrode junction is considered to be critically important.[11]

One of the main strategies to enhance the power conversion efficiency (PCE) is to engineer the electrode interface by the insertion of a buffer layer between the active layer and either the anode or the cathode.[12] To this purpose, various materials have been explored, such as metals (Ca, Ba),[13,14] salts (LiF, Cs_2CO_3),[15] organic materials and transition-metal oxides (Ti, Cr, Zn, Ni, oxides).[16-21]

Among them titanium oxides indeed hold great promise for the fabrication of different device structures, thanks to their unique electronic and optical properties. In particular crystalline nanostructured TiO_2 synthesized by established synthetic routes[22,23] has been commonly used as *n*-type material for photovoltaic applications, in dye-sensitized solar cells (DSSC)[24,25] and polymer/TiO_2 hybrid solar cells.[26,27] Recently, solution-processed of nonstoichimetric titanium oxide (TiO_X) has been exploited as an optical spacer, oxygen barrier and electron-transporting/hole-blocking (ETL/HBL) layer in the fabrication of conventional and inverted organic solar cell geometries.[20,28-30] The preparation of such material involves the sol-gel reaction of metal alkoxide precursors and thermal annealing at 100°C in ambient atmosphere to generate amorphous TiO_X. This thermal treatment in the presence of oxygen results in the degradation of OPV active materials; therefore, a simple coating process of TiO_2 without the requirement of the additional annealing step in air is deemed necessary.[31] In addition, due to

their amorphous nature, most of the reported TiO_X layers exhibit relatively low carrier mobility compared with their crystalline counterparts.[32] On the other hand, to obtain crystal phases, such as the anatase and rutile polymorphs, the TiO_X films must undergo a crystallization process upon annealing at temperatures of at least 400°C.[21] The necessity such harsh treatment disqualifies the use of TiO_X for the implementation of polymer solar cells with printed plastic electronics technologies.

Recent works have reported some attempts toward the insertion of a thin layer of colloidal hydrophobic-capped crystalline TiO_2 nanorods (NRs) in between the photoactive material and the cathode.[33,34] The elongated structure of NR shaped TiO_2 lead to a more efficient charge transport.[35] The drawback of this approach is that the photoactive organic layer is partially dissolved and damaged by the nonpolar solvents, such as toluene and chloroform, in which the NRs are efficiently dispersed and manipulated for device fabrication.[33]

In this work we have explored a novel strategy that enables straightforward utilization of colloidal anatase TiO_2 NRs into both conventional and inverted solar cell geometries with improved performances. To this aim we have exploited the concomitant mechanisms of UV-light-driven hydrophylicization of TiO_2 surfaces and photocatalytic demolition of surface-adsorbed organic species to create high-quality nanocrystalline TiO_2 thin films suitable for integration and operation in polymer photovoltaic devices. In one approach to inverted cells, UV-light treatment performed directly on pre-existing NR solid films deposited from nonpolar colloidal solution (e.g., toluene, chloroform) of surfactant-stabilized NRs guarantees good transport properties upon removal of the native insulating capping from the nanocrystals without altering the morphological features of the films. In an alternative route to conventional cells, UV irradiation shined onto hydrophobic NR solutions leads to organic-free, hydrophilic TiO_2 NRs readily dispersible in polar solvents, (i.e. methanol), which can be then processed into smooth and homogeneous TiO_2 nanocrystal films deposited onto polymer film without damaging or affecting the morphology of the organic layer underneath. Our study reports a detailed characterization of such TiO_2 NR films and discusses their successful exploitation as key functional components in organic photovoltaic cells.

Experimental

Materials. All chemicals were used as received. Titanium tetraisopropoxide [$Ti(OPri)_4$ or TTIP, 97%], trimethylamine *N*-oxide dihydrate [$(CH_3)_3NO{\cdot}2H_2O$ or TMAO, 98%] and oleic acid ($C_{17}H_{33}CO_2H$ or OLAC, 90%) were purchased from Aldrich. Silicon wafers were purchased from Jocam. All solvents used were of analytical grade and were also purchased from Aldrich. Water was bidistilled (Millipore Q).

Synthesis of TiO_2 nanorods (NRs). All syntheses were carried out under nitrogen flow using a standard Schlenk line set-up. Oleate-capped anatase TiO_2 nanorods (NRs) were obtained by low-temperature TMAO-catalyzed hydrolysis of TTIP in OLAC at 100°C.[36] The NRs were separated from their growing mixture upon 2-propanol addition and were subsequently subjected to repeated cycles of re-suspension in toluene and precipitation with acetone to wash out surfactant residuals. The as-purified NRs were fully dispersible in nonpolar solvents, such as chloroform ($CHCl_3$), dichloromethane (CH_2Cl_2), tetrachloromethane (CCl_4), tetrahydrofurane (THF), toluene, hexane, and cyclohexane, providing optically clear solutions. Organic TiO_2 nanocrystal stock solutions in different solvents (henceforth referred to as “dispersing solvents”) were prepared at a concentration of 0.5 M (expressed in terms of TiO_2 molecular units).

Preparation of organic-free TiO_2 Film Coatings on ITO substrates. TiO_2 NR coatings were fabricated under ambient laboratory conditions as follows. A solution of purified TiO_2 NRs in $CHCl_3$ was spin-coated onto ITO cleaned substrates at 1500 rpm for 60s to form a TiO_2 layer of *ca.* 25nm. The TiO_2 coatings were irradiated with a continuous wave-UV (cw-UV) lamp (SPECTROLINE E-Series Ultraviolet hand Lamps with excitation wavelength centered at 365 nm and energy density of 1 mW cm^{-2}) positioned at a distance of 5 cm from the sample.

Under these conditions, the organic coating was photocatalytically removed in less than *ca.* 100 min, as supported by the disappearance of all relevant infrared absorption bands of the OLAC capping layer. Afterwards, chlorobenzene was dispensed on top of the film and then spun-cast to remove possible organic residuals (undetectable by FTIR), followed by a gentle heating at T=120°C to remove the solvent. This protocol constituted one cycle of the ‘sequential spin-casting’ procedure to fabricate a robust TiO_2 film of *ca.* 100nm.

UV-driven hydrophilicization of the TiO_2 NRs in solution. In a typical experiment, a *ca.* 3 mL of a TiO_2 stock solution of purified TiO_2 NRs in $CHCl_3$ was put in a closed quartz-glass cuvette under air and was irradiated with the cw-UV lamp positioned at a distance of 15 cm from the sample. Upon irradiation, the precipitated TiO_2 was centrifuged, and washed twice with fresh $CHCl_3$. Finally, the TiO_2 NRs resulted in being dispersible in methanol. The TiO_2 concentration was determined ICP-AES measurements.

Characterization of TiO_2 nanocrystals and films thereof. The concentration of the TiO_2 solution was determined by digesting calibrated amounts of dry nanocrystals in concentrated HNO_3 and measuring the Ti content by inductively coupled plasma atomic emission spectroscopy (ICP-AES) measurements performed with a Varian Vista AX spectrometer.

Low-magnification transmission electron microscopy (TEM) images of TiO_2 NRs were recorded with a JEOL JEM 1011 microscope operating at an accelerating voltage of 100 kV. The samples for TEM analyses were prepared by dropping dilute TiO_2 solutions onto carbon-coated copper grids and then allowing the solvent to evaporate.

Fourier Transform Infrared (FTIR) spectroscopy measurements in the 4000-400 cm^{-1} spectral range were carried out on TiO_2 films deposited on silicon substrates using a JASCO FT-IR 6300 spectrophotometer in transmission mode at a resolution of

4 cm^{-1}. The surface topography of the TiO_2 films was investigated by acquiring AFM images with a Park Scanning Probe Microscope (PSIA) operating in tapping mode. The films for AFM investigations were prepared following the same procedure as that used for device measurements. Film thickness was measured by using an Alfa-Step IQ profilometer.

Fabrication and Testing of Solar Cells. ITO glass substrates were sequentially cleaned by ultrasonication in deionized water, acetone and 2-propanol, than were cleaned for 10 min at 85°C using TL-1 solution cleaner. For the inverted structure a blended solution of poly(3-hexylthiophene) (P3HT, Rieke Metals):[6,6]- phenyl-C_{61}-butyric acid methyl esther (PCBM, Nano-C) (1:0.8 wt % in CB) was spin-coated at 700 rpm for 45 s and dried under a Petri dish on the TiO_2 film prepared as described in the previous section. The obtained film was annealed at 110°C for 10 min. To complete the device structure, a thin layer of MoO_3 (*ca.* 7 nm) and an Al electrode (*ca.* 100 nm) were thermally evaporated at low pressure ($<1\times10^{-6}$ Torr). For the fabrication of conventional devices, a *ca.* 40 nm thin layer of PEDOT: PSS (H. C. Stark, CLEVIOS) was spin-coated onto the cleaned ITO substrates, followed by baking on a hot plate at 140°C for 15 min, under N_2 atmosphere in a glove box. The blended solution of P3HT:PCBM was prepared under the same conditions as the inverted device. By varying the concentration of the blended solution, active layers with variable thickness of 60±5, 80±5 and 110±5 nm, respectively, were achieved. The obtained film was annealed at 110°C for 10 min. Afterwards, the TiO_2 NR solution was spin-coated on P3HT:PCBM at a rate of 700 rpm for 100 s to obtain a film of *ca.* 15 nm, followed by a gentle annealing at 120°C for 10 min in the glove box (with H_2O<1ppm). An Al electrode (ca. 100 nm) was thermally evaporated at low pressure ($<1\times10^{-6}$ Torr). The metal electrodes have been deposited through a shadow mask. In order to limit shadowing effect and to render the metal thickness homogeneous, the shadow mask has been placed in contact with the device and the sample holder has been mounted on a rotating stage. The active area of the device has been accurately determined by optical microscope, using a 4× magnification objective equipped with a ruler. The active area of *ca.* 0.03 cm^2 was obtained. For comparison, devices without TiO_2 buffer layer were also prepared using similar fabrication conditions. Current density versus voltage (J-V) measurements was carried out under ambient conditions, keeping the illuminated light intensity fixed to 100 mW/cm^2.

Result and Discussion

1. UV-treatments on TiO_2 Nanorods

1.1 Post-deposition UV-treatment. TEM images in Fig. 1a reveal that the TiO_2 NRs are 20–40 nm in length and 4–5 nm in diameter. The as-synthesized TiO_2 NRs were capped with an insulating organic layer of deprotonated OLAC anions with long alkyl chains exposed outwards.

To prove the effectiveness of our treatment, the TiO_2 films were examined by FT-IR analysis. Fig. 1b shows the infrared spectra in the region 4000-800 cm^{-1} of the as-prepared TiO_2 NRs film (black trace) and after post-deposition UV irradiation (red trace).

The IR spectrum of the untreated film displays characteristic narrow absorption bands at 2930 and 2850 cm^{-1}, which correspond to the antisymmetric and symmetric C-H stretching vibrations, respectively, of the -CH_2- moieties of the hydrocarbon chains.[36,37]

Below 2000 cm^{-1}, two characteristic bands centred at *ca.*1530 and *ca.*1440 cm^{-1}, respectively, are associated with the COO- antisymmetric and symmetric stretching vibrations of carboxylate groups coordinated with surface Ti centers; the lack of clear evidence for the free C=O stretching band of free (protonated) OLAC molecules at around 1710-1720 cm^{-1} and the frequency difference of the aforementioned carboxylate bands confirm that the OLAC ligands are mostly bound to the TiO_2 surface through forming bidendate coordination complexes.[36,38] The broad absorption centred at *ca.* 3400 cm^{-1} of the irradiated film can be ascribed to the stretching vibrations of O-H groups associated with water adsorbed both molecularly and dissociatively (terminal Ti-O–H moieties), which originates from UV-driven surface reaction and reconstruction processes in the presence of atmospheric water.[36,38] It can be noted that after UV irradiation the bands relative to the OLAC ligands are no longer observable, thus confirming that the removal of the carboxylic ligands from the TiO_2 surface has actually occurred.

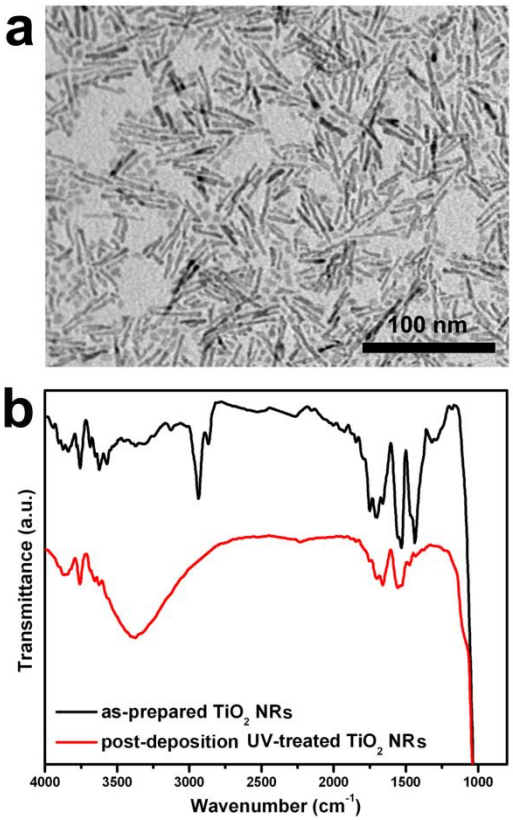

Fig.1 a) Low-resolution TEM image of as-synthesized Anatase TiO_2 NRs. b) FT-IR spectrum of as-synthesized TiO_2 NRs (black trace) and of post-deposition UV-treated TiO_2 NRs (red trace) on silica substrate (the spectra have been normalizated to the TiO_2 transmittance at 754 cm^{-1}).

The AFM images of the metal-oxide (Fig. S1a and S1b supporting information) show the topography of films made of the spin coated NRs before and after the post deposition UV treatment, respectively. In both cases the surface of the TiO_2-cathode was homogeneous and flat, with a very low root-mean-square (rms) surface roughness (*ca.* 1.5 nm). Moreover, complete substrate coverage without any cracks was achieved over areas as large as several squared micrometers, indicating that the UV-treatment did not alter the morphology of the as-deposited film. For a proper device operation, it is critically important to realize a very evenly flat TiO_2 substrate onto which to deposit the required organic layers. Apart from these film requirements, it is also very important to prevent formation of leakage paths to the ITO underneath.

1.2 UV-treatment on colloidal solution. The as-synthesized and purified TiO_2 NRs, dissolved in $CHCl_3$ or toluene, were subjected to UV irradiation. During the course of irradiation, the solution became turbid due to massive nanocrystal flocculation, which indicated loss of the initial hydrophobic character due to photocatalytic removal of the surface-bound oleate ligands. Such UV-flocculated TiO_2 NRs, collected by centrifugation, were then found to be re-dispersible in polar solvents (e.g. methanol, ethanol, 2-propanol, ACN, etc.), ultimately providing colloidal NR solutions with long-term stability and good optical transparency.

Fig. 2a compares the FT-IR spectra of the as synthesized TiO_2 NRs and after UV-irradiation in solution deposited on silica substrate.

It can be noted that after UV illumination all the vibrational bands relative to the OLAC ligands were highly suppressed, which demonstrates that most of the organic ligands have been removed from the NR surface, whereas it is evident that the degree of NR surface hydroxylation had significantly increased, as evidenced by the broad –OH stretching band in the 3600-3100 cm^{-1} region. Although the presence of some OLAC carboxylate residuals could not be excluded completely, the TiO_2 surface coverage appeared to be dominated by hydroxyl moieties, similar to what has been found for solid films of subjected to UV-irradiation treatment (Fig. 1b). The process that lead to the transition from highly hydrophobic to highly hydrophilic TiO_2 NRs is induced by both the loss of organic hydrophobic surfactant and by the hydroxylation of the NRs surface.The overall increased hydrophilicity of the TiO_2 NR surface is consistent with their changed solubility behavior after the UV treatment in the liquid phase.

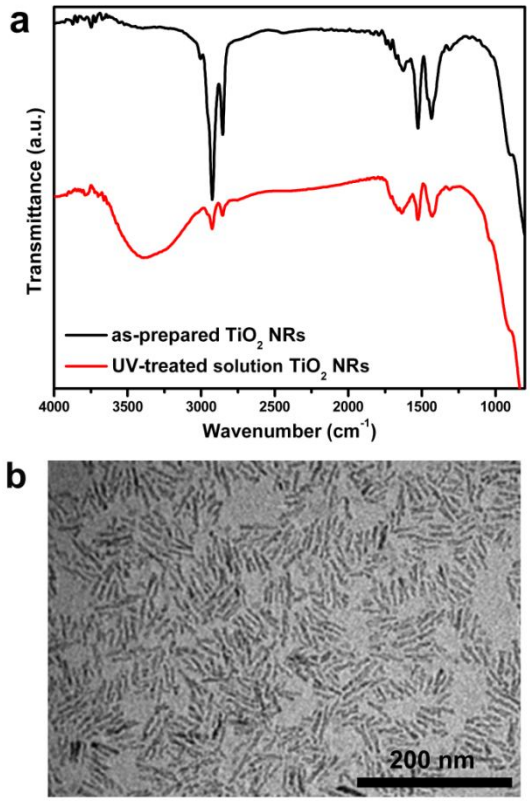

Fig.2 a) Normalized FT-IR spectrum of as-synthesized TiO_2 NR (black trace) and after UV-treatment (red trace) in solution (the spectra have been normalizated to the TiO_2 transmittance at 754 cm^{-1}). b) Representative low-resolution TEM images of TiO_2 NRs after UV-treatment in solution.

TEM (Fig. 2b) and AFM (Fig. S1c, Supporting Information) inspections of the UV-treated NRs deposited from the methanol solution revealed nanocrystals with unaltered size and shape parameters and negligible tendency toward agglomeration both on nanometer and micrometer scale. The AFM topography image (Fig. S1c) shows surface features smaller than a few nanometers and rms surface roughness value of 1.5 nm on an area of 5x5 μm^2. Achieving films with good morphological properties is a stringent requirement for such buffer layers to work as optical spacers. The extremely smooth and homogeneous morphology of our NR films, which can be attributed to the high processability of the UV-hydrophilicized NRs in polar media, fulfills all these requirements. The hydrophilicization of the TiO_2 after the exposure to the UV-light has been proven by measuring the contact angle (Fig. S2, supporting information) of the film before, *ca.* 100°, and after, *ca.* 20°, the irradiation.

2. TiO_2 based Solar cells

2.1 Photovoltaic Devices with Inverted Geometry. In order to study the effect of the UV-treatment of the TiO_2 in film on the performance of polymeric solar cells, an inverted device geometry was realized.

In general, in an inverted-device configuration, indium tin oxide (ITO), covered with a low work-function compound, functions as the cathode, while the anode is built up on the opposite side with a high-work-function electrode. The polarity of the device can thus be controlled by the relative positions of these functional layers with different work functions. Owing to the large band gaps and matching energy levels, titanium oxide (work function *ca.* 4.3 eV, LUMO *ca.* 4.4 eV) is also suitable as functional interfacial layer, since it can block hole collection on the ITO side, thus inverting the polarity of the devices. The growing interest in inverted devices originates from some recent studies which demonstrate that the use of metal oxides (TiO_X, ZnO) as the electron-collecting species can improve device stability under ambient conditions[40] and provide additional interfaces at which excitons can dissociate.[41]

The inverted layered structure of the device and the corresponding energy level diagram are sketched in Fig. 3a. After light absorption and exciton formation, charge separation occurs at the interface between the donor, P3HT, and the acceptor, PCBM. The photogenerated electrons diffuse through the TiO_2 film and are collected at the ITO, while the holes diffuse through the hole-extracting buffer MoO_3 and are collected at the Al cathode.

A reference inverted device without any treatment applied to the TiO_2 cathode (device A), was fabricated. We have

compared devices fabricated by our method (device B) with those realized by the standard process, in which a sintering step is generally introduced to remove the organic ligands; a reference device by means of sintering-treatment (device C) was fabricated.

The measured J-V characteristics of the three devices under illumination and in the dark are shown in Fig. 3b. The photovoltaic performance of these devices are summarized in Table 1.

Under AM 1.5 G illumination at 100 mW/cm^2, for the reference device A with no treatment, the open circuit voltage is V_{OC} = 0.53 V, the short circuit current is J_{SC} = 4.95 mA/cm^2, the fill factor is FF = 27%, and PCE = 0.7%, whereas device B exhibited an overall improvement in the device parameters with V_{OC} = 0.64 V, J_{SC} = 7.21 mA/cm^2, FF = 50%, and PCE = 2.3%. The reached PCE represents a *ca.* three times improvement over the unmodified device A.

The slope of the dark J-V curve of the device B with UV treatment near 0 V was lower than that of the device A without any treatment, leading to an increase in FF. The UV treatment thus made positive impact in improving the electron-transporting characteristics. Indeed, upon removal of the insulating surfactant from the TiO_2 NR surface by the UV treatment, the device B showed FF = 50%, which is two times higher than the FF of the untreated device A. Additionally, both J_{SC} and V_{OC} were enhanced by the insertion of the UV-treated TiO_2 NRs between the active layer and the cathode. The series resistance (R_s) and shunt resistance (R_{sh}), calculated from the inverse slope of J-V characteristics at V = 0V and V = V_{OC}, respectively, are shown in Table 1. The results indicate that the serial and shunt resistance of the devices could be largely improved through the interface modification devised by us. Compared to the inorganic-organic TiO_2/P3HT:PCBM interface in device A and B, elimination of the insulating surfactants from the TiO_2 layer drastically reduced the series resistance, which facilitated electron transport and thereby decreased the charge recombination losses through this interface.

The device C made by sintering-treatment showed a V_{OC} = 0.47V, J_{SC} = 5.56 mA/cm^2, FF = 41% and PCE = 1.1%, which are lower than that of device B. In particular the V_{OC} value is strongly dependent from the interface between the active layer and the electrodes.[12] For optimal device performance, it is critically needed that the different layers of the device stack are uniform and defect-free over large areas. This is difficult to accomplish in conventional devices that are subjected to sintering, as the stress caused in the film by the high-temperature annealing process generally leads to defect formation.[39] As a confirmation, the AFM images of TiO_2 films deposited and sintered as a single layer (*ca.* 25 nm) exhibit marked clustering among NRs which results in large clumps and voids (Fig. S3, Supporting Information). Recent studies have documented that, when ITO is used in devices, the fabrication of which involves high-temperature treatments, the electrical resistivity of the ITO tends to be increased.[42] It is plausible that the worse performance of the device C is due to both the lower surface quality of the TiO_2 cathode and the increase in the electrical resistivity of the ITO substrate, the latter accounting for the observed reduction in J_{SC}.

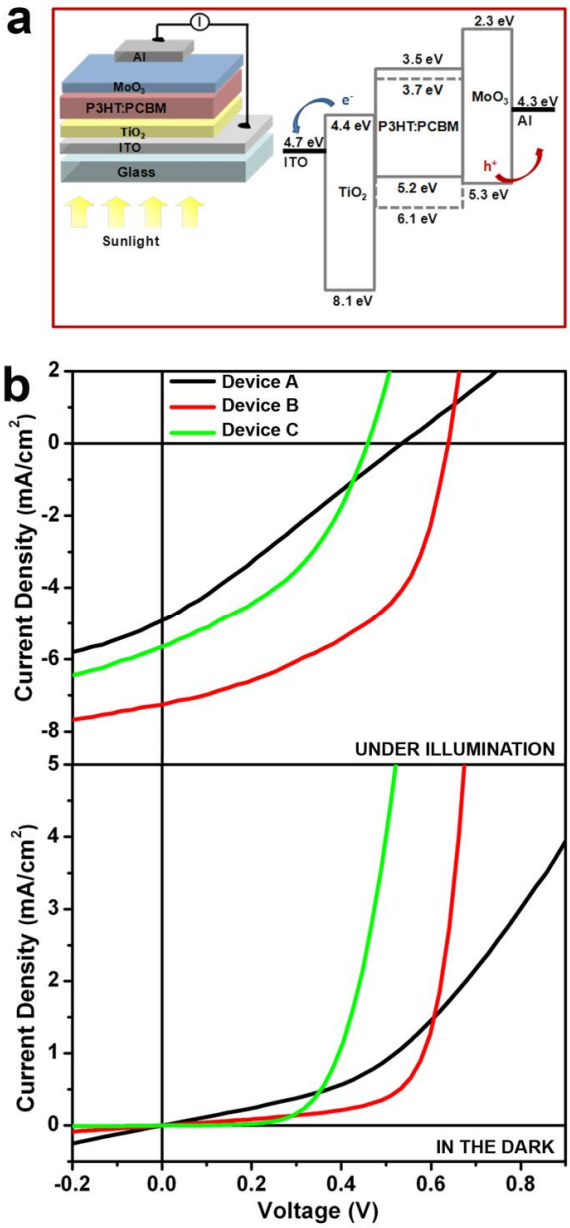

Fig.3 a) Schematic representation of the layered structure and energy level diagram for an inverted OPV device based on a ITO/TiO_2/P3HT:PCBM/MoO_3/Al configuration; b) Current density–Voltage characteristics under illumination and in the dark.

Table 1 Summary of Inverted Device Properties Prepared for different TiO_2-cathode.

Device	J_{SC}(mA/cm^2)	V_{OC}(V)	FF	PCE(%)	R_{sh}(Ωcm^2)	R_s(Ωcm^2)
Device A[a]	4.95	0.53	0.27	0.71	0.80×10^3	194.10
Device B[b]	7.21	0.64	0.50	2.31	0.26×10^4	19.66
Device C[c]	5.56	0.47	0.41	1.14	2.12×10^4	29.36

[a] No treatment [b] UV-treatment [c] Sintering-treatment.

2.2 Photovoltaic Devices with Conventional Geometry. To integrate TiO_2 NRs as a buffer layer in conventional solar cell geometry, a thin and smooth film of TiO_2 NRs has to be deposited onto the active layer. As explained in the previous section, the UV irradiation on colloidal solution of TiO_2 nanorods ultimately makes them redispersible in polar media, such as methanol, after precipitation and separation. In this way, the TiO_2 film could be deposited from solution onto the pre-existing layers by means of orthogonal solvents at room temperature. This is the first report in which the known mechanism of UV-light-driven hydrophilicization of TiO_2 has been purposely exploited for the fabrication of organic photovoltaic devices entirely made via low-temperature solution processing of colloidal TiO_2 nanocrystals.

The active layer was not damaged by the polar methanol and only a gentle annealing (T= 120°C) was made to remove the solvent. This gentle annealing could be carried out in controlled nitrogen atmosphere to prevent the polymer layer from oxidation; this is advantageous over other methods, which instead require an annealing step in air atmosphere.[28,29] The layered structure of the device and the corresponding energy level diagram are schematically shown in Fig. 4.

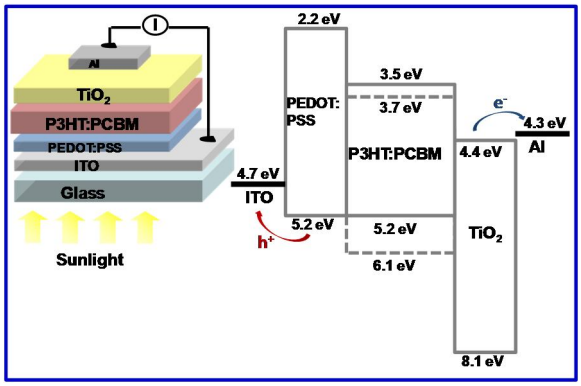

Fig.4 Schematic representation of the layered structure and energy level for a conventional OPV device, i.e. ITO/PEDOT: PSS/P3HT: PCBM/TiO_2/Al.

The coating TiO_2 layer well fulfills the requirements as electron-transporting layer (ETL) and hole-blocking layer (HBL). Indeed the lowest-unoccupied molecular orbital (LUMO) level of TiO_2 (4.4 eV) matches well with the Fermi level of Al (4.3 eV) and facilitates electron transfer from PCBM (LUMO level: 3.7 eV) to Al. Concurrently, the high energy of the highest-occupied molecular orbital (HOMO) level (8.1 eV) of TiO_2 prevents hole accumulation at the active layer/cathode (Al) interface, which leads to reduced probability of interfacial charge recombination.

The AFM topography and phase images of the blend thin films with and without TiO_2 NRs coating are reported in Fig. S4 (Supporting Information).

Importantly, the active layer coated by the TiO_2 NRs exhibited a smooth morphology and a root-mean-square (rms) surface roughness value *ca.* 1.5 nm. The TiO_2 layer conformed to the profile of the polymer blend without destroying it and without forming aggregates (Fig. S4a, S4b). The comparison of the phase images in Fig. S4c and S4d highlights that the TiO_2 completely covered the polymer active layer.

In a BHJ solar cell with the structure glass/ITO/PEDOT: PSS/BHJ/TiO_2/Al, the light incident upon the device from the glass side travels through the nearly transparent ITO and PEDOT: PSS layers, is partly absorbed by the photoactive BHJ layer, passes through the nearly transparent TiO_2 layer and is then reflected at the aluminum surface for a second pass through the BHJ, PEDOT: PSS, and ITO layers. Since TiO_2 does not absorb in the visible and infrared (Fig. S5, Supporting Information), it modifies the interference between the incident and reflected waves, thereby shifting the position of maximum intensity. The optical-spacer concept implies that a judicious choice of optical spacer thickness and index of refraction will cause the position of the maximum intensity to fall within the BHJ thin film and, consequently, increase the overall absorption and photocurrent. This enhancement is not only determined by the thickness and the optical constants (refractive index and extinction coefficient) of the optical spacer but also by the thickness and optical constants of all the other layers within the BHJ solar cell, including ITO, PEDOT:PSS, and the BHJ material.

In order to gain quantitative insight the working of TiO_2 NRs as optical spacer, we performed simulations of the optical-field distribution for 550 nm light illumination, corresponding to the peak absorption wavelength of P3HT:PCBM active layer, in devices with variable BHJ thickness (110 nm and 60 nm) and fixed thickness of the other layers. The results of the simulations are reported in Fig. 5. If considering the device with a thicker active layer (Fig. 5a), the interference effect between the incident and reflected light was suppressed because most of the incident light was absorbed. This result suggests that the use of an optical spacer in BHJ films with thickness about 110 nm or higher may not lead to large gains in J_{SC}. The simulation of the thinner active layer (Fig. 5b) revealed that the use of the TiO_2 optical spacer could indeed lead to an increase in the absorption, in agreement with previous reports.[43]

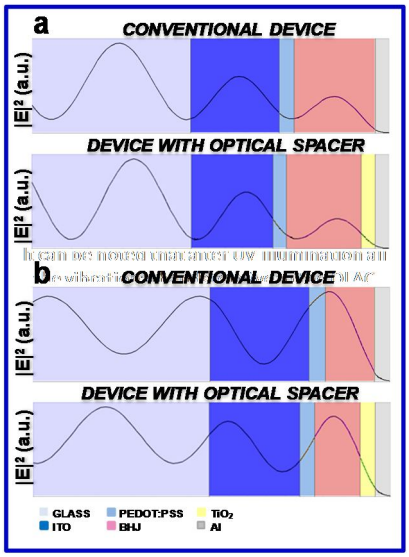

Fig.5 Schematic representation of the spatial distribution of the squared optical electric field strength $|E|^2$ inside the devices with a structure of ITO/PEDOT/BHJ/Al (up) and ITO/PEDOT/ BHJ/ TiO_2/Al (under) for two different thickness of active layer: a) 110 nm and b) 60 nm.

In order to confirm the effect of TiO_2 buffer layer as optical spacer on the OPV device performances, BHJ films with different thicknesses were prepared: 110 nm (device D), 80 nm (device E) and 60 nm (device F).

In Fig. 6 the current-voltage characteristics of devices D, E and F with and without TiO_2 layer under A.M. 1.5 illumination and the relative incident-photon-to-current efficiency (IPCE) measurements are plotted. The photovoltaic performances are summarized in Table 2.

Incorporation of TiO_2 buffer layer increased the shunt resistance by more than an order of magnitude, while lowering R_s by *ca.* 22-48%. The reduction in R_s correlated well with the enhancement in J_{SC}.[44,45] The improved R_{sh} suggested that the TiO_2 buffer layer prevented the charge from escaping from the cathode to the active layer, e.g. at the pinhole regions, which ultimately resulted in decreasing the leakage current of devices.

The saturation current density (J_0) could be extrapolated by fitting ($V-JAR_s$) versus $\ln(J-(V-JAR_s)/AR_{sh})$ from the y-axis intercept.

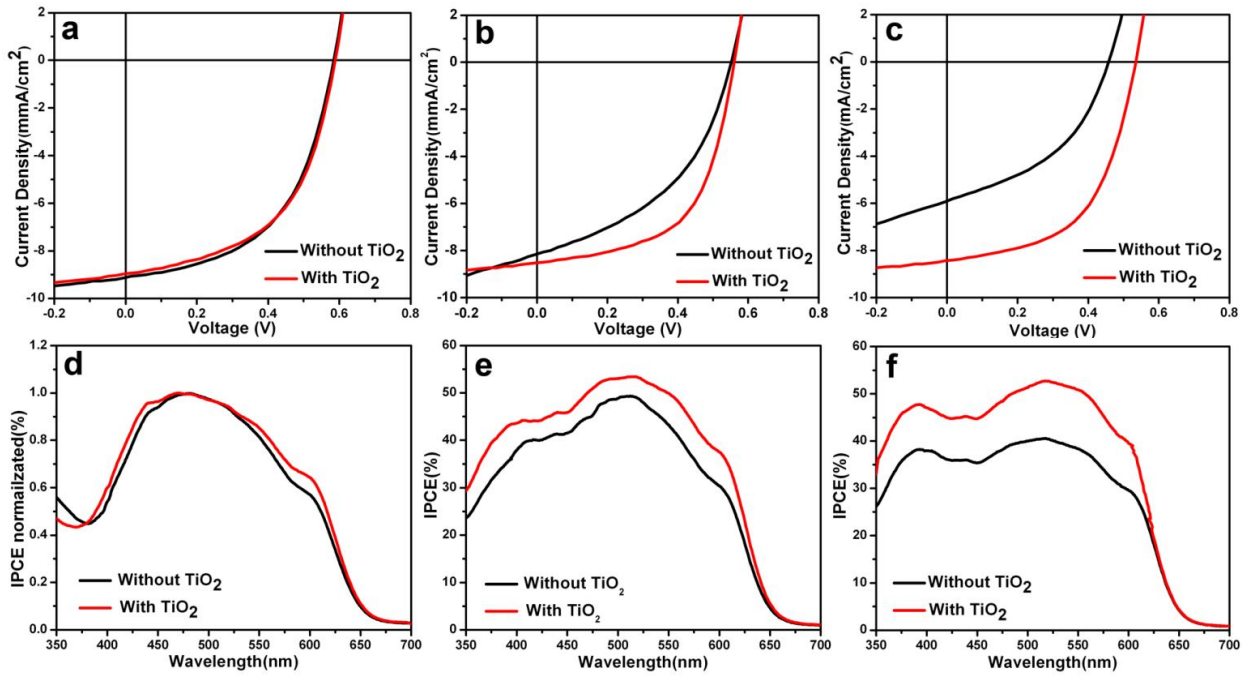

Fig.6 Current density- voltage curves of conventional OPV devices with different active layer thickness of (a) 110nm (device D), (b) 80 nm (device E), (c) 60 nm (device F), and the respective IPCE curve (d) 110nm (device D), (e) 80 nm (device E), and (f) 60 nm (device F).

With the TiO_2 layer between the active layer and the aluminum cathode electrode, the J_0 decreased by an order of magnitude for the device E and by more than an order of magnitude for the device F. The HOMO level of the TiO_2 layer is much lower in energy than the HOMO levels of P3HT or PCBM (see scheme in Fig. 4). For this reason, the insertion of the TiO_2 layer was expected to reduce the hole carrier contribution to the current density and therefore to reduce the J_0. We considered the decreased J_0 to be an indirect evidence for the fact that TiO_2 indeed served as a hole-blocking layer in a BHJ solar cell. The increase in open circuit voltage was a direct outcome of the hole-blocking effect of TiO_2, and the increase in FF implied a higher maximum power point current as a result of delayed turn-on of current injection due to the hole-blocking.

Table 2. Summary of Conventional Device Properties Prepared with and without TiO_2.

Device	TiO_2	J_{SC}(mA/cm^2)	V_{OC}(V)	FF	PCE(%)	R_{sh}(Ωcm^2)	R_s(Ωcm^2)	J_0(A/cm^2)
Device D[a]	No	9.08	0.58	0.53	2.79	8.47×10^{4}	28.21	8.53×10^{-9}
Device D[a]	Yes	8.94	0.60	0.52	2.79	3.21×10^{5}	20.16	4.77×10^{-9}
Device E[b]	No	6.67	0.53	0.59	2.09	2.72×10^{3}	25.20	2.48×10^{-7}
Device E[b]	Yes	8.50	0.55	0.58	2.74	1.79×10^{5}	19.61	6.30×10^{-8}
Device F[c]	No	5.82	0.47	0.43	1.16	0.31×10^{3}	47.22	1.03×10^{-4}
Device F[c]	Yes	8.40	0.53	0.55	2.46	0.29×10^{5}	24.43	7.52×10^{-7}

Active layer thicknesses: [a] 110nm, [b] 80 nm and [c] 60 nm.

The IPCE is defined as the number of photogenerated charge carriers contributing to the photocurrent per incident photon. For the device E, maximum IPCE at 514 nm are 49% and 54% for the devices with and without TiO_2 buffer layer, respectively. In this case, the improvement in IPCE with TiO_2 buffer layer was low, suggesting that TiO_2 did not play a role as optical spacer in device with a thick active layer. While for the device F with an active layer of 60 nm, the results demonstrated a substantial enhancement in the IPCE by *ca.* 30% over the entire excitation spectral range for the device with TiO_2. Integration of the IPCE spectra over the visible spectrum corresponded well to the difference in J_{SC} of the devices. We attributed this enhancement to an increased light absorption in the bulk heterojunction layer as a result of the TiO_2 optical spacer action; the enhanced photogeneration of charge carriers resulted from the spatial redistribution of the light intensity. Moreover, the Fig. 6d shows the normalized IPCE spectra of the device D with and without TiO_2. Although the TiO_2 layer did not lead to a large gain in J_{SC} (Fig. 6a), the shape of the curve notably changed due to an optical spacer effect, which is in good agreement with the simulations.

The expected enhancement in absorption due to the TiO_2 layer as optical spacer in thinner devices was additionally confirmed by reflectivity measurements. In Fig. S6 (Supporting Information), we show the plot of the ratio of the reflected light versus the wavelength in devices with and without TiO_2 to calculate the enhancement in absorption due to the TiO_2 layer as optical spacer. Since the two devices fabricated were identical except for the presence of the TiO_2 optical spacer, a comparison of the respective reflectance provided information on the change in absorption, □□□□), in the P3HT: PCBM composite film as a result of the spatial redistribution of the light intensity by the TiO_2 layer. The data demonstrate a clear increase in absorption over the spectral region of the interband transitions, which results in an increase of the number of carriers per incident photon collected at the electrodes.

Conclusions

In summary, we have demonstrated two different approaches to improve the performance of polymer photovoltaic devices by the integration of anatase TiO_2 NRs. In the first approach we have exploited the post-deposition UV-treatment on TiO_2 NR films for the fabrication of inverted solar cells. In the second approach we exploited the integration of UV-irradiated NR solutions as electron-transporting/hole-blocking material and optical spacer in conventional device geometry.

The TiO_2 NRs were prepared through a simple colloidal synthesis and integrated as functional layer into devices without any additional hydrolysis process or harsh thermal sintering in the air. This allows maintenance of an inert environment during device fabrication. Through the successful integration in the photovoltaic devices and film characterizations, we have demonstrated that the our UV-treatments, both in film and in solution, gently remove the insulating organic ligand from the NR surface and ensure an optimized morphology and charge transport properties.

In particular we have reported that the inverted devices after the post deposition UV-treatment showed a PCE of 2.3% that is *ca.* three times improvement over their corresponding device counterpart incorporating untreated TiO_2.

In addition, we have demonstrated that the UV-driven TiO_2 hydrophilicization and photocatalytic removal of the ligands directly in solution phase, reverted the solubility behavior of the original TiO_2 nanocrystals. NRs redispersed in polar solvents were successfully used as buffer layer in conventional solar cells, which results in doubled PCE (2.46% vs 1.16%) for the 60 nm thick active layer devices. Our approach represents a simple and general method for the fabrication of optoelectronic devices, fully compatible with polymeric device technology, which is expected to facilitate the integration

of nanocrystalline TiO_2 into more complex and efficient solar cell architectures, such as multilayer, tandem and ITO-free devices.

[a] *Dipartimento di Ingegneria dell`Innovazione, Università del Salento, via per Arnesano, I-73100 Lecce, Italy*
[b] *Center for Bio-Molecular Nanotechnologies (CBN) of IIT@NNL-UniLe-Lecce, via Barsanti c/o STAMMS, Arnesano 73010 Lecce, Italy*
[c] *NNLCNR-, Istituto Nanoscienze, c/o Distretto Tecnologico, via per Arnesano Km.5, I-73100 Lecce, Italy*
[d] *Scuola Superiore ISUFI, Università del Salento, via per Arnesano, I-73100 Lecce, Italy*
** Corresponding author: Tel: 0039-0832-298211. Fax: 0039-0832-298237. E-mail: aurora.rizzo@nano.cnr.it.*

Acknowledgements
This work was supported by the Italian projects Rete Nazionale di Ricerca sulle Nanoscienze ItalNanoNet (FIRB reference number RBPR05JH2P) and EFOR—Energia da FOnti Rinnovabili (Iniziativa CNR per il Mezzogiorno L. 191/2009 art. 2 comma 44) and by the European project ESCORT- Efficient Solar Cells based on Organic and hybrid Technology (7th FWP—reference number 261920).

1 C. J. Brabec, N. S. Sariciftci, J. C. Hummelen, *Adv. Funct. Mater.* 2001, **11**, 15-26.
2 P. Peumans, S. Uchida, S. Forrest, *Nature*, 2003, **425**, 158-162.
3 B. C. Thompson, J. M. Frechet, *J. Angew. Chem.*, Int. Ed. 2008, **47**, 58-77.
4 F. C. Krebs, T. Tromholt, M. Jørgensen, *Nanoscale*, 2010, **2**, 873-886.
5 E. Bundgaard, F. C. Krebs, *Sol. Energy Mater. Sol. Cell* , 2007, **91**, 954.
6 R. Kroon, M. Lenes, J. C. Hummelen, P.W.M. Blom, B. De Boer, *Polym. Rev.*, 2008, **48**, 531.
7 J. Peet, M. L. Senatore, A. J. Heeger and G.C. Bazan, *Adv. Mater.*, 2009, **21**, 1521.
8 A. Hadipour, B. de Boer, P. W. M. Blom, *Adv. Funct. Mater.*, 2008, **18**, 169.
9 J. Y. Kim, K. Lee, N. E. Coates, D. Moses, T. Q. Nguyen, M. Dante, A. J. Heeger, *Science*, 2007, **317**, 222.
10 L.-M. Chen, Z. Hong, G. Li and Y.Yang, *Adv. Mater.*, 2009, **21**, 1434-1449.
11 H. Ma, H. L. Yip, F. Huang and A. K. Y. Jen, *Adv. Funct. Mater.*, 2010, **20**, 1371–1388.
12 Z. He, C. Zhong, X. Huang, W.Y. Wong, H. Wu, L. Chen, S. Su and Y. Cao, *Adv. Mater.*, 2011, DOI: 10.1002/adma.201103006.
13 Y. S. Eo, H. W. Rhee, B. D. Chin and J.-W. Yu, *Synth. Met.*, 2009, **159**, 1910-1913.
14 M. O. Reese, M. S. White, G. Rumbles, D. S. Ginley and S. E. Shaheen, *Appl. Phys. Lett.*, 2008, **92**, 053307-3.
15 L. S. Hung, R. Q. Zhang, P. He and G. J. Mason, *J. Phys. D:Appl. Phys.*, 2002, **35**, 103.
16 J. Huang, Z. Yinb and Q. Zheng, *Energy Environ. Sci.*, 2011, **4**, 3861-3877.
17 M. Wang, Q. Tang, J. An, F. Xie, J. Chen, S. Zheng, K. Y. Wong, Q. Miao and J. Xu, *ACS Appl. Mater. Interfaces*, 2010, **2**, 2699-2702.
18 A. Gilot, I. Barbu, M. M. Wienk, and R. A. J. Janssen, *Appl. Phys. Lett.*, 2007, **91**, 113520-3.
19 M. D. Irwin, D. B. Buchholz, A. W. Hains, R. P. H. Chang and T. J. Marks, *Proc. Natl. Acad. Sci. U.S.A.*, 2008, **105**, 2783-2787.
20 S. K. Hau, Y.-J. Cheng, H.-L. Yip, Y. Zhang, H. Ma and A. K. Y. Jen, *ACS Appl. Mater. Interfaces*, 2010, **2**, 1892-1902.
21 T. Kuwabara, C. Iwata, T. Yamaguchi and K. Takahashi, *ACS Appl. Mater. Interfaces*, 2010, **8**, 2254-2260.
22 X. Chen and S. S. Mao, *Chem. Rev.*, 2007, **107**, 2891-2959.
23 L. Song, Y. M. Lam, C. Boothroyd and P. W. Teo, *Nanotechnology,* 2007, **18**, 135605.
24 U. Bach, D. Lupo, P. Comte, J. E. Moser, F. Weissortel, J. Salbeck, H. Spreitzer and M. Gretzel, *Nature*, 1998**, 395**, 583**.**
25 O. R. Brian, M. Gretzel, *Nature*, 1991, **353**, 737–740.
26 A. C. Arango, L. R. Johnson, V. N. Bliznyuk, Z. Schlesinger, S. A. Carter and H. H. Horhold, *Adv. Mater.*, 2000, **12**, 1689.
27 P. A. van Hal, M. M. Wienk, J. M. Kroon, W. J. H. Werhees, L. H. Slooff, W. J. H. Gennip, P. Jonkheijm amd R. A. J. Janssen, *Adv. Mater.,* 2003, **15**, 118.
28 S. H. Park, A. Roy, S. Beaupre, S. Cho, N. Coates, J. S. Moon, D. Moses, M. Leclerc, K. Lee and A. J. Heeger, *Nat. Photon.*, 2009*,* **3**, 297-302.
29 J. Li, S. Kim, S. Edington, J. Nedy, S. Cho, K. Lee, A.J. Heeger, M.C. Gupta and J.T.Y. Jr, *Solar Energy Materials & Solar Cells*, 2011, **95**, 1123-1130.
30 C. Tao, S. Ruan, X. Zhang, G. Xie, L. Shen, X. Kong, W. Dong, C. Liu and W. Chen, *Appl. Phys. Lett.,* 2008, **93**, 193307.
31 M. H. Park, J. H. Li, A. Kumar, G. Li and Y. Yang, *Adv. Funct. Mater.*, 2009, **19**, 1241-1246.
32 J. H. Park, T. W. Lee, D. Chi, D. H. Wang and O. O. Park, *Macromol. Rapid Commun.*, 2010, **31**, 2095-2108.
33 T. W. Zeng, Y. Y. Lin, H. Lo, C. W. Chen, C. H. Chen, S. C. Liou, H. Y. Huang and W. F. Su, *Nanotechnology*, 2006, **17**, 5387-5392.
34 Y. Y. Lin, T. H. Chu, S. S. Li, C. H. Chuang, C. H. Chang, W. F. Su, C. P. Chang, M. W. Chu and C.W. Chen, *J. Am. Chem. Soc.*, 2009, **131**, 3644-3649.
35 S. Dayal, M.O. Reese, A.J. Ferguson, D.S. Ginley, G. Rumbles, N. Kopidakis, *Adv. Funct. Mater.*, 2010, **20**, 2629-2635.
36 (a) G. Caputo, C. Nobile, T. Kipp, L. Blasi, V. Grillo, E. Carlino, L. Manna, R. Cingolani, P. D. Cozzoli and A. Athanassiou, *J. Phys. Chem. C*, 2008, **112**, 701-714. (b) G. Caputo, B. Cortese, C. Nobile M. Salerno, R. Cingolani, G. Gigli, P.D. Cozzoli and A. Athanassiou, *Adv. Funct. Mater.*, 2009, **18**, 1149-1157; (c) G. Caputo, R. Cingolani, P.D. Cozzoli and A. Athanassiou, *Phys. Chem. Chem. Phys.*, 2009, **11**, 3692-3700.
37 R. M. Silverstein and F. X. Webster, *In Spectrometric Identification of Organic Compounds*, Sixth Ed.; John Wiley & Sons, Inc., 1997.
38 P. D. Cozzoli, A. Kornowski and H. Weller, *J. Am. Chem. Soc.*, 2003, **125**, 14539.
39 Q. Guo, G. M. Ford, H. W. Hillhouse and R. Agrawal, *Nano Lett.*, 2009, **9**, 3060-3065.
40 S. K. Hau, H. L. Yip, N. S. Baek, J. Zou, K. O'Malley and A. K. Y. Jen, *Appl. Phys. Lett.*, 2008, **92**, 253301.
41 D. A. Bernards, T. Biegala, Z. A. Samuels, J. D. Slinker, G. G. Malliaras, S. F. Torres, H. D. Abruna and J. A. Rogers, *Appl. Phys. Lett.*, 2004, **84**, 3675.
42 G. H. Guai, Q. L. Song, Z. S. Lu and C. M. Li, *Surface & Coatings Technology*, 2011, **205**, 2852-2856.
43 A. Roy, S. H. Park, S. Cowan, M. H. Tong, S. Cho, K. Lee and A. J. Heeger, *Appl. Phys. Lett.*, 2009, **95**, 013302.
44 M.-S. Kim, B.-G. Kim, J. Kim, *ACS Appl. Mater. Interfaces*, 2009, **1**, 1264-1269.
45 J. D. Servaites, S. Yenageh, T. J. Marks, M. A. Ratner, *Adv. Funct. Mater.*, 2010, **20**, 97-104